LARGE AMPLITUDE WAVE PROPAGATION IN ARTERIES AND VEINS

Y. KIVITY[†] and R. COLLINS[‡]

1. INTRODUCTION

The problem of finite amplitude wave propagation in fluid-filled distensible tubes, although of potentially wide general interest in industrial piping systems, finds particularly important application in biomedical circulatory phenomena. Mathematical and laboratory studies of such coupled fluid-shell interactions have led to novel contributions in the field of Biomechanics, an area of continuing activity in the United States and England, and one which is rapidly attracting the attention of scientists and medical researchers in France.

The pulsatile flow of blood from the heart into the aorta, and subsequently the connecting great vessels, engenders wave propagation in the vessel walls, the motion of which in turn modifies the blood flow. This interaction between fluid and vessel wall motions will depend strongly upon the material properties of the system, such as fluid density and viscosity and the dynamic viscoelastic properties of the wall, in addition to the mechanical contraints imposed on the vessel by the surrounding connective tissue and intercostal arteries. Pathologically-induced changes in these properties will be evidenced in modified pressure and flow variations in the distal portions of the arterial system. Alternatively, such variations may serve as a basis for estimating such changes in the material properties.

Although radial excursions of 8-10 % of the aortic lumen have been generally observed in in situ measurements under normal physiological conditions, little if any longitudinal displacements of the vessel wall have been detected. A recent study by Kivity and Collins (1973) describes a numerical method for determining instantaneous variations in vessel cross-section, pressure and fluid velocity under conditions of complete longitudinal tethering. However, in laboratory testing of excised biological specimens, large longitudinal motions of the wall are known to occur.

---

† On leave from the Scientific Department, Ministry of Defense Israel.

‡ On sabbatical leave from University of California, School of Engineering and Applied Science, Los Angeles, U.S.A.

The present work provides a generalized treatment of viscous fluid motion in a nonlinear orthotropic viscoelastic thin walled tube. A numerical solution is described based upon a two-step Lax-Wendroff finite difference scheme which is shown to be very stable and rapid.

2. MATHEMATICAL FORMULATION

2.1 Physical Relations

In this present generalized treatment of the axisymmetric motion of an incompressible fluid in a nonlinear viscoelastic tube, the fluid viscosity is accounted for and hence the action of wall friction on longitudinal displacements of the vessel wall. The actual wall-thickness to diameter ratio of the human aorta is about one-tenth. Under the thin wall approximation, this ratio is considered insignificantly small, leading mathematically to neglect of the shear stresses and bending moments. Patel and Fry (1969) showed that the aorta and carotid arteries developed shearing strains that were very much smaller than the corresponding longitudinal and circumferential strains, when the vessel was inflated to physiological pressures. Thus the vessel is orthotropic, and shear strains can be neglected. In this case, the three orthogonal strains : circumferential, longitudinal and radial are the only important ones. For an incompressible wall (Poisson ratio equals one-half), they are interrelated.

A large deflection theory for thin shells of revolution has been given by Reissner (1949) and a more generalized treatment is described in the book by Krauss (1967). Under the foregoing assumptions, the equilibrium of an element of the shell is expressed by Reissner's Eq. (28) as

$$\frac{\partial}{\partial \xi}\left(r N_\xi \vec{J}_\xi\right) + \frac{\partial}{\partial \theta}\left(\alpha N_\theta \vec{J}_\theta\right) + r\alpha \vec{p} = 0 \qquad (1)$$

where ξ is a Lagrangian coordinate along the generator of the middle surface of the tube, θ is the polar angle of a point on the middle surface (see figs. 1 and 2) and x , y , z are the corresponding Eulerian coordinates, $r = (x^2 + y^2)^{1/2}$ is the Eulerian coordinate of a point on the generator of the surface and must be regarded as functions of (ξ , t) since the problem is time dependent.

α is defined by

$$\alpha^2 = \left(\frac{\partial r}{\partial \xi}\right)^2 + \left(\frac{\partial z}{\partial \xi}\right)^2 \qquad (2)$$

N_ξ and N_θ are the stress resultants in the ξ and θ directions, $\vec{p}$ is the load intensity vector (external load per unit area).

In the context of the theory of shells, the load $\vec{p}$ is usually specified. In the present problem, however, the load $\vec{p}$ results from the interaction between the fluid and the tube. The wall motion is hence coupled to that of the fluid through the load vector $\vec{p}$ per unit area. A number of external forces contribute to the load intensity vector $\vec{p}$. The normal component p_n arises from the fluid hydrodynamic pressure acting normal to the inner layer of the wall, in addition to possible normal forces imposed on the outer layer by visceral resistance to radial motions. The tangential component p_ξ derives from the shear stress τ due to viscous drag at the inner wall, as well as from longitudinal restraints on the outer wall associated with the "tethering" effects of connective tissue and intercostal arteries (Patel and Fry 1966).

The quasi one-dimensional viscous flow equations for an incompressible fluid in a distensible axi-symmetric duct may be expressed as :

$$\text{(continuity)} \; : \; \frac{\partial}{\partial t} r^2 + \frac{\partial}{\partial z}\left(r^2 v\right) = 0 \qquad (3)$$

$$\text{(momentum)} \; : \; \frac{\partial}{\partial t} v + \frac{\partial}{\partial z}\left(\frac{v^2}{2} + p_{hydro}/\rho + \phi\right) = -F \qquad (4)$$

where v is the fluid velocity (averaged over the cross-section), ρ is the constant density of the fluid, $p_{hyd.}$ is the hydrostatic pressure which is equal but of opposite sign to the normal component of the external load p_n and ϕ the gravitational force potential defined by

$$\frac{\partial \phi}{\partial z} = G \qquad \text{(acceleration)}$$

F represents the friction per unit mass of fluid due to viscous fluid drag at the wall. For circular tubes

$$F = \frac{2}{\rho R} \tau \qquad (5)$$

where τ is the shear stress at the wall.

For steady flow in a pipe, from the corresponding formulae of Poiseuille and Blasius (Schlichting 1968, p. 79 and 561) for laminar and turbulent flow, one obtains the shear stress

$$\tau = c_f \tfrac{1}{2} \rho v^2 Re^{-m} \qquad (6)$$

where the Reynolds number $Re = \rho R|v|/\mu$,

c_f is the dimensionless skin friction coefficient, and μ is the fluid viscosity.

For laminar flow $m = 1$ and $c_f = 8$, while for turbulent flow $m = 1/4$ and $c_f \cong .07$.

In the present calculations, the laminar form of the shear stress has been used, corresponding to the generally accepted principle that turbulent regions are rare in most normal physiological blood flows. For example, it was pointed out by Ling et al (1968) that according to hot-film anemometric measurements carried out in the arteries of living animals, the flow is normally nonsteady and laminar. That is, flow profiles are developed locally and transiently during the passage of each pulsatile wave. The rise time of the pressure-gradient wave front is of the order of 0.02 seconds (under normal physiological conditions) and the apparent propagating velocity of the wave front is approximately 600 cm/sec., implying a physical width of the travelling wave of about 12 cm. In general, flow profiles were found to be blunt and axially symmetric. Both turbulence and secondary flows were found to be inhibited and localized by the nature of the pulsatile flow, and although weak turbulence was observed in the aortic arch of small dogs, it was quickly dissipated within each heart cycle.

Nonetheless, in the regions near the shock front where conditions are clearly not physiological, such may no longer be the case. Although these expressions are strictly valid only for steady flow, they will be applied here for the unsteady flow conditions to be described subsequently.

To complete the system of equations (1), (3), (4) one must add a constitutive relation linking wall stresses to strains and rates of strain within the vessel wall. For this purpose, a mathematical expression relating the stress resultants N_ξ and N_θ to the material coordinates ξ, z and their time derivatives would be desirable. However, even for small deformations, such a highly developed constitutive relation is not presently available without mentioning the still greater lack of knowledge for the large deformation, high strain-rate range corresponding to shock experiments.

A simplified material model is proposed in which the stress is related to strain and strain-rate in the circumferential and longitudinal directions separately. This effectively decoupled representation is not inconsistent with the assumption of orthotropy implicit in the thin-walled approximation described above.

Physically, this representation of the state of stress corresponds to a model of the tube wall composed of two distinct layers : a layer of "fibers", which carries the stress in the tangential direction and a layer of "rings", which carries the hoop stress. Similar ideas have been put forth by Apter et al. (1966).

The stress strain-rate relation in each direction is written in the form

$$\sigma(\lambda, \dot{\lambda}) = f(\lambda) + g(\lambda, \dot{\lambda}) \qquad (7)$$

with

$$g(\lambda, 0) = 0 \qquad (8)$$

so that $f(\lambda)$ represents the static loading relation. As a measure of strain, the extension ratio is employed here, with

$$\lambda = L/L_0 \qquad (9)$$

where L is the length of a strained element and L_o is its length at some reference state. For the measurements of Collins and Hu (1972), the explicit expression (7) becomes

$$\sigma(\lambda, \dot{\lambda}) = E\left(1 + B\,\dot{\lambda}/\lambda\right)\left(\lambda^n - 1\right) \qquad (10)$$

with $n = 12$, $B = 0.64$ sec. and $E = 0.28 \times 10^6$ dynes/cm^2 along the axial direction.

Relation (10) may be converted to an expression for the stress resultants in terms of the coordinates r , z . The circumferential extension is simply

$$\lambda_\theta = \frac{r(\xi, t)}{r(\xi, 0)} = \frac{r}{r_o} \qquad (11)$$

The axial extension may be expressed in terms of the quantity α of Eq. (2) by

$$\lambda_\xi = \frac{\alpha(\xi, t)}{\alpha(\xi, 0)} = \frac{\alpha}{\alpha_o} \qquad (12)$$

the stress resultants are then related to the stresses by

$$N = h\sigma \qquad (13)$$

where h is the wall thickness. The variations of the wall thickness h with the tube displacements may be found in a simple manner if one uses the Poisson ratio $\nu = 1/2$ typical of biological tissue. In this case, the material is incompressible, so that

$$\frac{\partial}{\partial t}(r \alpha h) = 0$$

or

$$r(\xi, t)\,\alpha(\xi, t)\,h(\xi, t) = r_o(\xi)\,\alpha_o(\xi)\,h_o(\xi) \qquad (14)$$

where

$$f_o(\xi) = f(\xi, t=0)$$

Equations (1), (3), (4) and (10) and their associated relations, constitute a complete system governing the coupled fluid-wall motions.

In the next section, these will be reduced to a simpler set, whose numerical solution, with illustrative values of the physical parameters, will be described in the remainder of the work.

2.2 Reduction of Governing Equations

It is convenient to decompose the vector equation (1) into its components in the ξ and n directions. These directions refer to the generator of the middle surface (see fig. 1). The hydrostatic pressure in the fluid contributes to the normal component p_n of $\vec{p}$ and the wall friction (due to fluid viscosity) to the tangential component p_ξ of $\vec{p}$ .Carrying out the differentiations in (1) gives

$$\frac{\partial}{\partial \xi}(r N_\xi)\vec{J}_\xi + \alpha N_\theta \frac{\partial}{\partial \theta}\vec{J}_\theta + r\alpha p_\xi \vec{J}_\xi + r N_\xi \frac{\partial}{\partial \xi}\vec{J}_\xi + r\alpha p_n \vec{J}_n = 0$$

Let $\vec{i}, \vec{j}, \vec{k}$, be unit vectors in the x, y and z directions respectively (see fig. 1). The radial and circumferential unit vectors $\vec{J}_r$ and $\vec{J}_\theta$ are then related to the former by (Reissner 1949) :

$$\vec{J}_r = \vec{i}\cos\theta + \vec{j}\sin\theta \; ; \quad \vec{J}_\theta = -\vec{i}\sin\theta + \vec{j}\cos\theta \qquad (15)$$

and the tangential and normal unit vectors by

$$\vec{J}_\xi = \vec{J}_r\cos\varphi + \vec{k}\sin\varphi \; ; \quad \vec{n} = -\vec{J}_r\sin\varphi + \vec{k}\cos\varphi \qquad (16)$$

Then from Eq. (16), one finds

$$\frac{\partial}{\partial \xi}\vec{J}_\xi = \vec{J}_n \frac{\partial \varphi}{\partial \xi} \qquad (17)$$

and from Eq. (15)

$$\frac{\partial}{\partial \theta}\vec{J}_\theta = -\vec{J}_r = -\vec{J}_\xi\cos\varphi + \vec{J}_n\sin\varphi \qquad (18)$$

where $\vec{j}_\varphi$ denotes a unit vector in the φ direction, and φ is the angle between the tangent to the meridian curve and the z-axis, with

$$\tan\varphi = \frac{\partial z/\partial \xi}{\partial r/\partial \xi} \tag{19}$$

The scalar components of Eq.(1) in the ξ and n - directions are now readily found to be :

$$\frac{\partial}{\partial \xi}(r N_\xi) - \alpha N_\theta \cos\varphi + r\alpha p_\xi = 0 \tag{20}$$

$$r N_\xi \frac{\partial \varphi}{\partial \xi} + \alpha N_\theta \sin\varphi + r\alpha p_n = 0 \tag{21}$$

For convenience, one replaces the variables N_ξ and N_θ by

$$T_\xi \equiv r N_\xi = \frac{r_o h_o \alpha_o}{\alpha} \sigma_\xi = r_o h_o \sigma_\xi / \lambda_\xi \tag{22}$$

$$T_\theta \equiv \alpha N_\theta = \frac{r_o h_o \alpha_o}{r} \sigma_\theta = \alpha_o h_o \sigma_\theta / \lambda_\theta \tag{23}$$

The scalar wall equations (20) and (21) then become

$$\frac{\partial}{\partial \xi} T_\xi - T_\theta \cos\varphi + r\alpha p_\xi = 0 \tag{24}$$

$$T_\xi \frac{\partial \varphi}{\partial \xi} + T_\theta \sin\varphi + r\alpha p_n = 0 \tag{25}$$

One can eliminate p_n $(= -p_{hydro})$ between Eqs. (4) and (25), yielding

$$N_t + \left\{ \frac{v^2}{2} + \frac{1}{\rho r \alpha}\left[T_\xi \frac{\partial \varphi}{\partial \xi} + T_\theta \sin\varphi \right] + \Phi \right\}_z + \frac{2}{\rho r}\tau = 0 \tag{26}$$

The governing system then reduces essentially to the three simultaneous equations (3), (24) and (26) in conjunction with the auxiliary relations (2), (5), (6), (10)-(14), (19), (22) and (23). p_ξ is the sum of all tangential loads acting on the wall; in the absence of tethering, $p_\xi = \tau$, the shear stress due to fluid viscosity.

2.3 Initial Boundary Value Problem

The system of Eqs. (3), (24), and (26) is solved numerically with the following illustrative boundary and initial conditions corresponding to an arterial segment open at one end ($\xi = 0$) with an applied stagnation pressure at the other end ($\xi = L$); that is :

$$\text{At } \xi = 0 \quad : \quad \begin{cases} p = 0 & \text{(open end)} \\ T_\xi = 0 & \text{(tube unrestrained longitudinally)} \end{cases} \qquad (27)$$

$$\text{At } \xi = L \quad : \quad P/\rho + \tfrac{1}{2} v^2 = H \begin{cases} \sin^2(\pi/2\, t) & \text{for } t < 20\,ms \\ 1 & \text{for } t \geq 20\,ms \end{cases} \qquad (28)$$

$$\text{and } Z = \text{Const.} = Z_0(L)$$

where ρH is constant and equal to the stagnation pressure in the reservoir

$$\text{At } t = 0 \quad : \quad \left.\begin{aligned} v(\xi, 0) &= 0 \\ A(\xi, 0) &= A_0(\xi) \\ Z(\xi, 0) &= Z_0(\xi) \end{aligned}\right\} \qquad (29)$$

2.4 Stability Considerations

The numerical stability of the set of governing equations may be assessed in approximate form, in a manner similar to that of Kivity and Collins (1973). That is,the system may be cast in both hyperbolic and parabolic forms, and the appropriate stability criteria developed for each. However, it has been confirmed in subsequent calculations that it is invariably the stability criterion associated with the parabolic form which is more restrictive, and hence only the derivation of that form is outlined here.

One considers the system of equations (3), (24) and (26) with the assumption, for simplicity, that $\phi = 0$ and $\tau = 0$. Then Eq (24) becomes

$$\frac{\partial T_\xi}{\partial \xi} = T_\theta \cos\varphi \; ; \quad T_\xi = \int T_\theta \cos\varphi \, d\xi + \text{Const.} \qquad (30)$$

Multiplying Eq(3) by v and Eq(28) by $A=\lambda^2$ and adding, one obtains, in terms of a new variable defined by $Q = Av$,

$$Q_t + \left(\frac{Q^2}{A}\right)_z + A\left[\frac{1}{\rho\lambda\alpha}\left(T_\xi \frac{\partial\varphi}{\partial\xi} + T_\theta \sin\varphi\right)\right]_z = 0 \qquad (31)$$

For small displacements, φ is very close to $\pi/2$, so that $\sin\varphi \cong 1$. Also, from (30), the change in T_ξ is small compared to T_θ, so that T_ξ is approximately a constant. The quantity $\frac{1}{\alpha}\frac{\partial\varphi}{\partial\xi}$, appearing in Eq(31), equals the curvature ($1/R_\xi$), and is also very small, under the above assumption, so that the term $T_\xi \frac{\partial\varphi}{\partial\xi}$ may be neglected with respect to T_θ. Eq.(31) then becomes

$$Q_t + \left(\frac{Q^2}{A}\right)_z + A\left(T_\theta/\rho\lambda\alpha\right)_z = 0$$

T_θ may be expressed in terms of A and $\dot{A} = -Q_z$, using the stress-strain relationship (10) employed in this study. The resulting differential equation takes on the form

$$Q_t - S\,Q_{\xi\xi} + W = 0 \qquad (32)$$

where W is a function of lower order ξ-derivatives which do not enter into this first order estimate of a numerical stability criterion, and

$$S = \frac{f(\lambda\theta)}{\lambda_\theta^2}\,\frac{h_o}{r_o}\,\frac{B_\theta/2}{\rho\lambda_\xi}\Big/\left(\frac{\partial z}{\partial\xi}\right)^2, \qquad (33)$$

$$\frac{\partial z}{\partial\xi} \cong \lambda_\xi \qquad (34)$$

The stability criterion for the parabolic equation (32) is

$$S\Delta t/(\Delta\xi)^2 \le 1/2$$

which implies a time step

$$\Delta t < \frac{\rho\lambda_\xi^3\lambda_\theta^2}{B_\theta f(\lambda\theta)\,h_o/r_o}(\Delta\xi)^2 \qquad (35)$$

3. NUMERICAL SOLUTION

For the solution of the system (3), (24) and (26), one employs a numerical algorithm based on the two-step Lax-Wendroff difference scheme. In each step, the radius r and the particle velocity v are explicitly advanced in time, using the continuity equation (3) and the momentum equation (26), respectively. The new value of r serves to determine a new value of T_θ from the relation (23). T_ξ is then determined by integration of (24). Finally, z is computed implicitly, using a simple Newton method.

This procedure has proved to be reliable, provided that one observes the stability criterion (35). In the actual calculation Δt was taken as 0.8 times the right hand side of (35). The initial estimate for z in the Newton method was obtained from the value of z at the previous step.

The Langrandian coordinate ξ was chosen to be the initial coordinate of a point; that is $z(\xi,0) = \xi$. To simplify the presentation of the difference scheme, the following abbreviations are used :

DEFINITIONS

$$\delta^n_{j+1/2} = \frac{1}{2}\,\frac{\Delta t^n}{z^n_{j+1} - z^n_{j-1}} \quad ; \quad \delta^n_j = \frac{\Delta t^n}{z^n_{j+1/2} - z^n_{j-1/2}}$$

$$f^n_{j+1/2} = \frac{1}{2}\left(f^n_j + f^n_{j+1}\right) \quad \text{(unless a different definition is explicitly specified)}$$

$$\pi = \frac{1}{2}v^2 + \frac{1}{\rho r \alpha}\left\{T_\xi \frac{\partial \varphi}{\partial \xi} + T_\theta \sin\varphi\right\}$$

$$\pi^n_j = \frac{1}{2}\left(v^n_j\right)^2 + \frac{1}{\rho r^n_j \alpha^n_j}\left\{\left(T_\xi\right)^n_{j+1/2} \frac{\varphi^n_{j+1/2} - \varphi^n_{j-1/2}}{\Delta\xi} + \right.$$

$$\left. + \left(T_\theta\right)^n_j \sin\varphi^n_j \right\}$$

$$\pi_{j+1/2}^{n+1/2} = \frac{1}{2}\left(v_{j+1/2}^{n+1/2}\right)^2 + \frac{1}{\rho r_{j+1/2}^{n+1/2}\,\alpha_{j+1/2}^{n}}\left\{\frac{1}{2}\left[(T_\xi)_j^{n+1/2} + (T_\xi)_{j+1}^{n+1/2}\right]\cdot\frac{\varphi_{j+1}^{n}-\varphi_j^{n}}{\Delta\xi} + (T_\theta)_{j+1/2}^{n+1/2}\sin\varphi_{j+1/2}^{n}\right\}$$

$$\left(\alpha_{j+1/2}^{n}\right)^2 = \left\{\left(z_{j+1}^{n}-z_j^{n}\right)^2 + \left(r_{j+1}^{n}-r_j^{n}\right)^2\right\}/(\Delta\xi)^2$$

$$\left(\alpha_j^{n}\right)^2 = \frac{1}{2}\left(\alpha_{j+1/2}^{n} + \alpha_{j-1}^{n}\right)$$

$$\varphi_{j+1/2}^{n} = \arccos\left(\frac{r_{j+1}^{n}-r_j^{n}}{\alpha_{j+1/2}^{n}\,\Delta\xi}\right)$$

$$\varphi_j^{n} = \frac{1}{2}\left(\varphi_{j+1/2}^{n} + \varphi_{j-1/2}^{n}\right)$$

$$(\lambda_\theta)_j^{n} = \frac{r_j^{n}}{(r_c)_j} \quad ; \quad (\lambda_\xi)_{j+1/2}^{n} = \frac{\alpha_{j+1/2}^{n}}{(\alpha_c)_{j+1/2}} \,.$$

The difference scheme consists then of the following steps :

STEP I

$$(r^2)_{j+1/2}^{n+1/2} = (r^2)_{j+1/2}^{n} - \delta_{j+1/2}^{n}\left[(r^2 v)_{j+1}^{n} - (r^2 v)_j^{n}\right]$$

$$v_{j+1/2}^{n+1/2} = v_{j+1/2}^{n} - \delta_{j+1/2}^{n}\left[\pi_{j+1}^{n} - \pi_j^{n}\right] - \frac{\Delta t^{n}}{\rho r_{j+1/2}^{n}}\,\tau\left(v_{j+1/2}^{n}, r_{j+1/2}^{n}\right)$$

$$(T_\theta)^{n+1/2}_{j+1/2} = (h_0\alpha_0)_{j+1/2}\, \sigma_\theta\left(\lambda\theta^{n+1/2}_{j+1/2},\ \frac{\lambda\theta^{n+1/2}_{j+1/2} - \lambda\theta^{n}_{j+1/2}}{\frac{1}{2}\Delta t^n}\right) \Big/ \lambda\theta^{n+1/2}_{j+1/2}$$

$$(T_\xi)^{n+1/2}_{j+1} = (T_\xi)^{n+1/2}_{j} + \Delta\xi \left\{ T\theta^{n+1/2}_{j+1/2} \cos\varphi^{n}_{j+1/2} - \right.$$

$$\left. - r^n_j \alpha^n_j\, \tau(\nu^n_j, r^n_j) \right\}$$

To determine $z^{n+1/2}_{j+1/2}$, solve the following implicit equation for $(\lambda_\xi)^{n+1/2}_j$,

$$\sigma_\xi\left(\lambda\xi^{n+1/2}_j,\ \frac{\lambda\xi^{n+1/2}_j - \lambda\xi^{n}_j}{\frac{1}{2}\Delta t^n}\right) \Big/ \lambda\xi^{n+1/2}_j = (T_\xi)^{n+1/2}_j \Big/ (r_0 h_0)_j$$

where the function $\sigma_\xi(\lambda, \dot\lambda)$ gives the stress in terms of the extension λ_ξ and its time rate of change. Knowing $(\lambda_\xi)^{n+1/2}_j$, $z^{n+1/2}_{j+1/2}$ is found from the relation :

$$\left(z^{n+1/2}_{j+1/2} - z^{n+1/2}_{j-1/2}\right)^2 + \left(r^{n+1/2}_{j+1/2} - r^{n+1/2}_{j-1/2}\right)^2 = \left(\lambda\xi^{n+1/2}_j\, (\alpha_0)_j\right)^2$$

STEP II

$$(r^2)^{n+1}_j = (r^2)^n_j - \delta^{n+1/2}_j \left\{ (r^2 v)^{n+1/2}_{j+1/2} - (r^2 v)^{n+1/2}_{j-1/2} \right\}$$

$$v^{n+1}_j = v^n_j - \delta^{n+1/2}_j \left\{ \pi^{n+1/2}_{j+1/2} - \pi^{n+1/2}_{j-1/2} \right\} -$$

$$- 2\frac{\Delta t^n}{\rho\, r_{av}}\, \tau\left(\frac{v^{n+1/2}_{j+1/2} + v^{n+1/2}_{j-1/2}}{2},\ r_{av}\right)$$

where $r_{av} = \frac{1}{2}\left(r^{n+1/2}_{j+1/2} + r^{n+1/2}_{j-1/2}\right)$

$$T_{\theta j}^{n+1} = (h_0 \alpha_0)_j \, \sigma_\theta \left(\lambda_{\theta j}^{n+1}, \frac{\lambda_{\theta j}^{n+1} - \lambda_{\theta j}^{n}}{\Delta t^n} \right) \Big/ (\lambda_\theta)_j^{n+1}$$

$$T_{\xi\, j+1/2}^{n+1} = T_{\xi\, j-1/2}^{n+1} + \Delta\xi \left\{ T_{\theta j}^{n+1} \frac{r_{j+1/2}^{n+1/2} - r_{j-1/2}^{n+1/2}}{\alpha_j^n \Delta\xi} - \right.$$

$$\left. - r_{av} \alpha_j^n \tau \left(\frac{v_{j+1/2}^{n+1/2} + v_{j-1/2}^{n+1/2}}{2}, r_{av} \right) \right\}$$

To determine z_j^{n+1}, one first solves for $(\lambda_\xi)_{j+1/2}^{n+1}$ from the equation:

$$\sigma_\xi \left(\lambda_{\xi\, j+1/2}^{n+1}, \frac{\lambda_{\xi\, j+1/2}^{n+1} - \lambda_{\xi\, j+1/2}^{n}}{\Delta t^n} \right) \Big/ (\lambda_\xi)_{j+1/2}^{n+1} = (T_\xi)_{j+1/2}^{n+1} \Big/ (r_0 h_0)_{j+1/2}$$

then, z_j^{n+1} is determined from :

$$\left(z_{j+1}^{n+1} - z_j^{n+1} \right)^2 + \left(r_{j+1}^{n+1} - r_j^{n+1} \right)^2 = \left[\lambda_{j+1/2}^{n+1} (\alpha_0)_{j+1/2} \right]^2$$

The difference analogue of the boundary conditions (27) and (28) is as follows:

Open end

$$r_1^{n+1} = \text{Const} = r_0(0)$$

$$v_1^{n+1} = v_1^n - 2 \delta_{1\,1/2}^n \left(\pi_2^n - \pi_1^n \right) - 2 \frac{\Delta t^n}{\rho r_{1\,1/2}^{n+1/2}} \tau \left(v_{1\,1/2}^{n+1/2}, r_{1\,1/2}^{n+1/2} \right)$$

z_1^{n+1} is computed by the general procedure.

Fixed end (with applied stagnation pressure)

$$z_{im}^{n+1} = L \qquad \text{(vessel length)}$$

$$v_{im}^{n+1} = v_{im}^{n} - \delta_{im-1/2}^{n} \left(\pi_{im}^{n+1/2} - \pi_{im-1/2}^{n+1/2} \right) - \frac{2\Delta t^{n}}{\rho r_{im-1/2}^{n+1/2}} \tau \left(v_{im-1/2}^{n+1/2}, r_{im-1/2}^{n+1/2} \right)$$

where $\pi_{im}^{n+1/2}$ is computed from the given applied stagnation pressure as a function of time = $t^n + \frac{1}{2}\Delta t^n$.

Then, r_{im}^{n+1} is calculated by first solving the implicit equation for $(\lambda_\theta)_{im}^{n+1}$

$$\tau_\theta \left(\lambda_{\theta im}^{n+1}, \frac{\lambda_{\theta im}^{n+1} - \lambda_{\theta im}^{n}}{\Delta t^n} \right) \Big/ \left[(\lambda_\theta)_{im}^{n+1} \right]^2 =$$

$$= \left[\pi_{im}^{n+1} - \tfrac{1}{2} (v_{im}^{n+1})^2 \right] \rho (r_0)_{im} (h_0)_{im} \alpha_{im-1/2}^{n+1/2} \Big/ (\alpha_e)_{im-1/2} \Big/ \sin\varphi_{im-1/2}^{n+1/2}$$

Then

$$r_{im}^{n+1} = (r_0)_{im} (\lambda_\theta)_{im}^{n+1}$$

NOTE

In calculating the variables r and v, one progresses from $\xi = 0$ to $\xi = L$ ($i = 1$ to $i = im$); whereas in the calculation of λ_ξ and z one starts at the fixed end $\xi = L$, since z is prescribed there.

4. RESULTS AND DISCUSSION

Illustrative computations have been carried out for an aorta, considered as a nonlinear viscoelastic material with a dynamic constitutive stress-strain-strain-rate relation of the functional form Eq.(10). The physical parameters selected are noted in Table I below :

TABLE I

$E_\xi = E_\theta = 0.28 \times 10^6$ dyn/cm^2

$B_\xi = B_\theta = 0.16$ Sec.

$n_\xi = n_\theta = 12$

$\mu = 0$

$\rho = 1.05$ g/c.c.

$C_0 = 300$ cm/Sec. (sound speed in the aorta at zero transmural pressure)

$R_0(\xi) = 1$ cm

$H = 0.63 \times 10^6$ dynes/cm^2.

Fig. 3 shows the evolution of shape changes at 10mS intervals, with the shock wave progressing along the tube from right to left, as a function of the Lagrangian axial coordinate ξ . The end $\xi = 100$ cm is held fixed, while the remainder of the tube is free to move longitudinally, as depicted in fig. 4. Such longitudinal motion, although inhibited by tethering for vessels in situ, must be considered in in vitro laboratory experiments using excised tissue. The radial and longitudinal displacements vary smoothly but the demarcation between "shocked" and undisturbed regions of the vessel wall is quite evident. The axial distributions of fluid velocity in fig.5 resemble the shape changes of fig. 3. The pressure distribution in the tube, although not shown here, may be calculated directly from the variation of the extension ratio α in fig. 6 and from the distributions of longitudinal and circumferential wall stresses in figs. 7 and 8, respectively.

The computational method possesses wide generality, well beyond that implicit in the above calculational example. The present analysis, in addition to admitting large longitudinal motions of a tapered tube, also included the effects of fluid viscosity and orthotropicity of the vessel wall.

The influence of variations of these latter parameters is summarized in Table II below for the steady-state solution of flow in a tube of uniform cross-section obtained numerically from the unsteady solution as the asymptotic limit for long times. The velocity dz_e/dt of the distal end of the tube $\xi=0$ is calculated from a simple finite difference at times of 70 and 75 mS.

The steady-state shock speed U may also be estimated from the velocity of the distal end of the tube, in terms of the extension ratio λ In a small time interval Δt, the tube elongates in the region over which the shock has passed, by an amount equal to the strain $(=\lambda-1)$ multiplied by the speed U of the wave front, that is

$$\Delta z_e = (\lambda_\xi - 1)\, U \Delta t$$

or

$$U = \frac{1}{\lambda_\xi - 1} \frac{dz_e}{dt}$$

This estimate of U, which is indicated in Table II, agrees favorably with that computed from the full solution.

TABLE II

case n°	$-dz_e/dt$ cm/sec	λ_ξ	$-U$ cm/sec	Notes
0	250	1.242	1040	parameters as in Table I
1	185	1.175	1055	parameters as in Table I except $E_\xi = 2E_\theta$
2	316	1.317	1000	parameters as in Table I except $E_\xi = 1/2\ E_\theta$
3	250	1.245	1020	parameters as in Table I except $\mu = .05$ poise, laminar friction law
4	183	1.154	1190	parameters as in Table I except $B_\xi = 10\ B_\theta$

Upon comparing the extension ratio λ_ξ for cases 0 and 3, it would appear that the fluid viscosity, and consequent drag on the tube wall, are not significant, although this conclusion remains tentative until further examples are examined. This would indicate that the wall forces are much more important than viscous drag in determining longitudinal displacements. However, Table II brings out the considerable influence of the orthotropicity on the extension ratios. In fact, both changes in the axial wall elasticity E_ξ (cases 0, 1 and 2) and in the axial viscoelastic modulus $\mathcal{B}_\xi$ (cases 0 and 4) effect important changes in the extension ratio λ_ξ. The steady state shock velocity appears nonetheless relatively insensitive to such changes, with the exception of the viscoelastic parameter $\mathcal{B}_\xi$. It may well be possible to exploit the sensitivity of the wall elongation as an indirect measure of the circumferential or axial wall moduli of biological vessels subjected to rapidly changing loads.

5. CONCLUSIONS

A numerical method has been described for the calculation of the unsteady flow of an incompressible viscous fluid in a distensible tapered tube possessing orthotropic viscoelastic properties. The formulation is quite general, including the fluid-wall interaction, the tube wall being characterized as a thin shell with negligible bending moments.

Illustrative solutions have been presented for the biomedical phenomena of a pulsed flow of blood in an excised segment of human aorta, subjected to both radial and longitudinal deformations. The complete solution includes the time variations of wall shape, stresses, strains and fluid velocity, computed in conjunction with a realistic dynamic constitutive model for the aortic wall.

The example presented possesses an impulsive inlet flow sufficient to produce "shock-like" signals along the vessel wall. These sharp wave fronts do not endanger the inherent stability of the numerical two-step Lax-Wendroff scheme, provided that the stability criteria are properly observed.

REFERENCES

Apter, J.T., Rabinowitz, Cummings, D.H. (1966):
Correlation of Viscoelastic Properties of Large Arteries with Microscopic Structure, Circulation Res. 19 : 104 - 21

Collins, R., Hu, W.C.L. (1972) : Dynamic Deformation Experiments on Aortic Tissue, J. Biomechanics 5, 333-337

Kivity, Y., Collins, R.(1973) : Nonlinear Wave Propagation in Viscoelastic Tubes, J. Biomechanics (in press) - Vol 6, n° 6, Dec. 1973

Krauss, H. (1967) : Thin Elastic Shells, John Wiley, Chap. II

Ling, S.C., Atabek, H.B., Carmody, J.J. (1968) : Pulsatile flows in Arteries in Applied Mechanics, Proceedings of the 12th Int'l Congress of Applied Mechanics, Stanford University Aug. 26-31, 1968, pp. 227-291, Springer-Verlag (1969)

Patel, D.J., Fry, D.L. (1966) : Longitudinal tethering of Arteries in Dogs. Circulation Res. 19 : 1011-21

Patel, D.J., Fry D.L. (1969) : The Elastic Symmetry of Arterial Segments in Dogs, Circulation Res. 24 : 1-8

Reissner, E. (1949) On the theory of Thin Elastic Shells, in Reissner Anniversary Volume edited by Polytechnic Inst. of Brooklyn, J.W. Edwards Publisher, Ann Arbor, Michigan

Schlichting, H. (1968) : Boundary-Layer Theory, 6th edition (transl. by J. Kestin) Mc Graw-Hill, New York

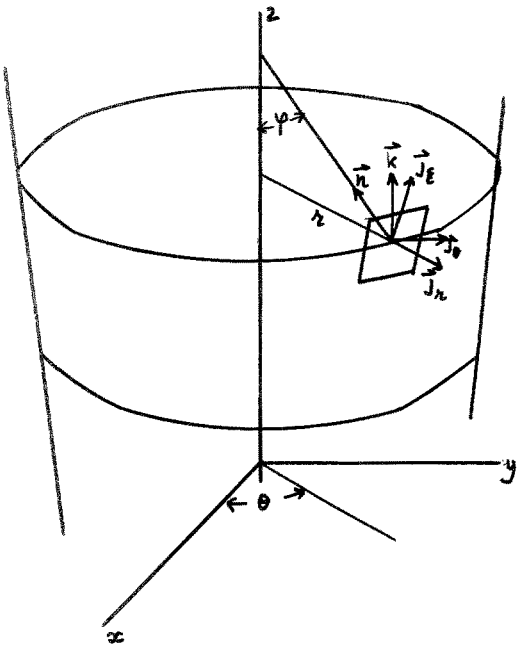

FIG. 1

MIDDLE SURFACE OF SHELL, SHOWING COORDINATES ξ, θ ON MIDDLE SURFACE AND UNIT VECTORS ASSOCIATED WITH MIDDLE SURFACE

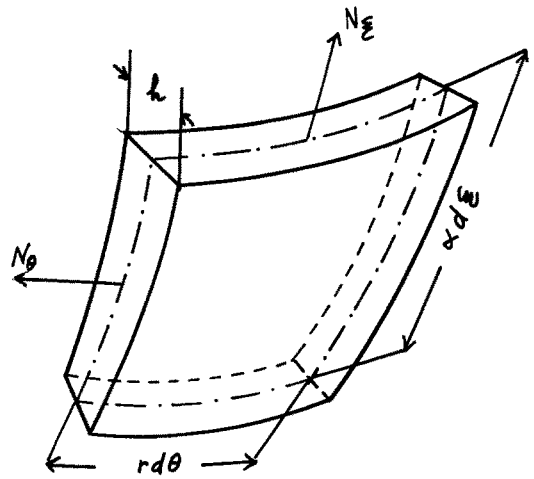

FIG. 2

ELEMENT OF SHELL SHOWING

STRESS RESULTANTS

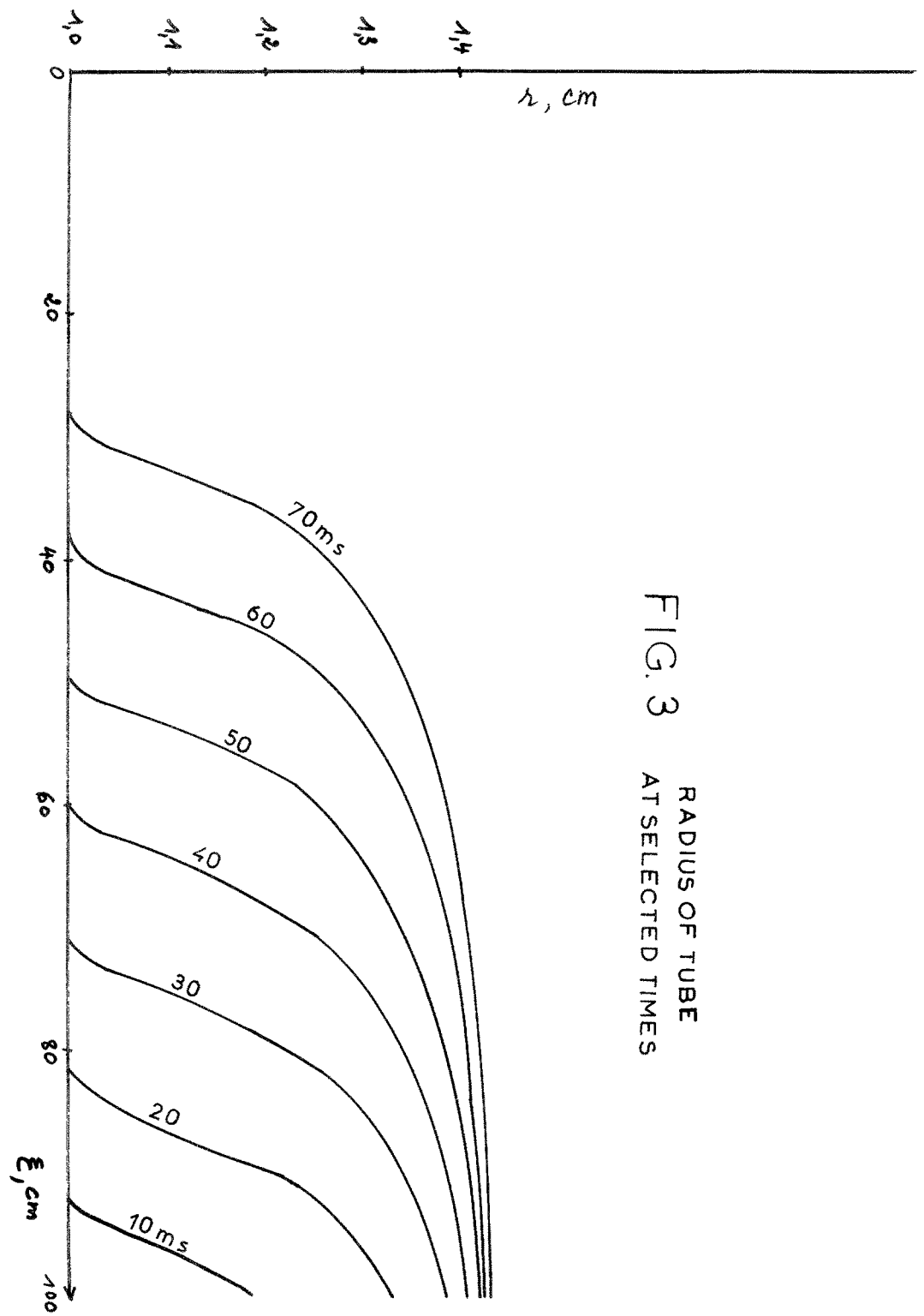

FIG. 3 RADIUS OF TUBE AT SELECTED TIMES

FIG. 4

AXIAL WALL DISPLACEMENT

AT SELECTED TIMES

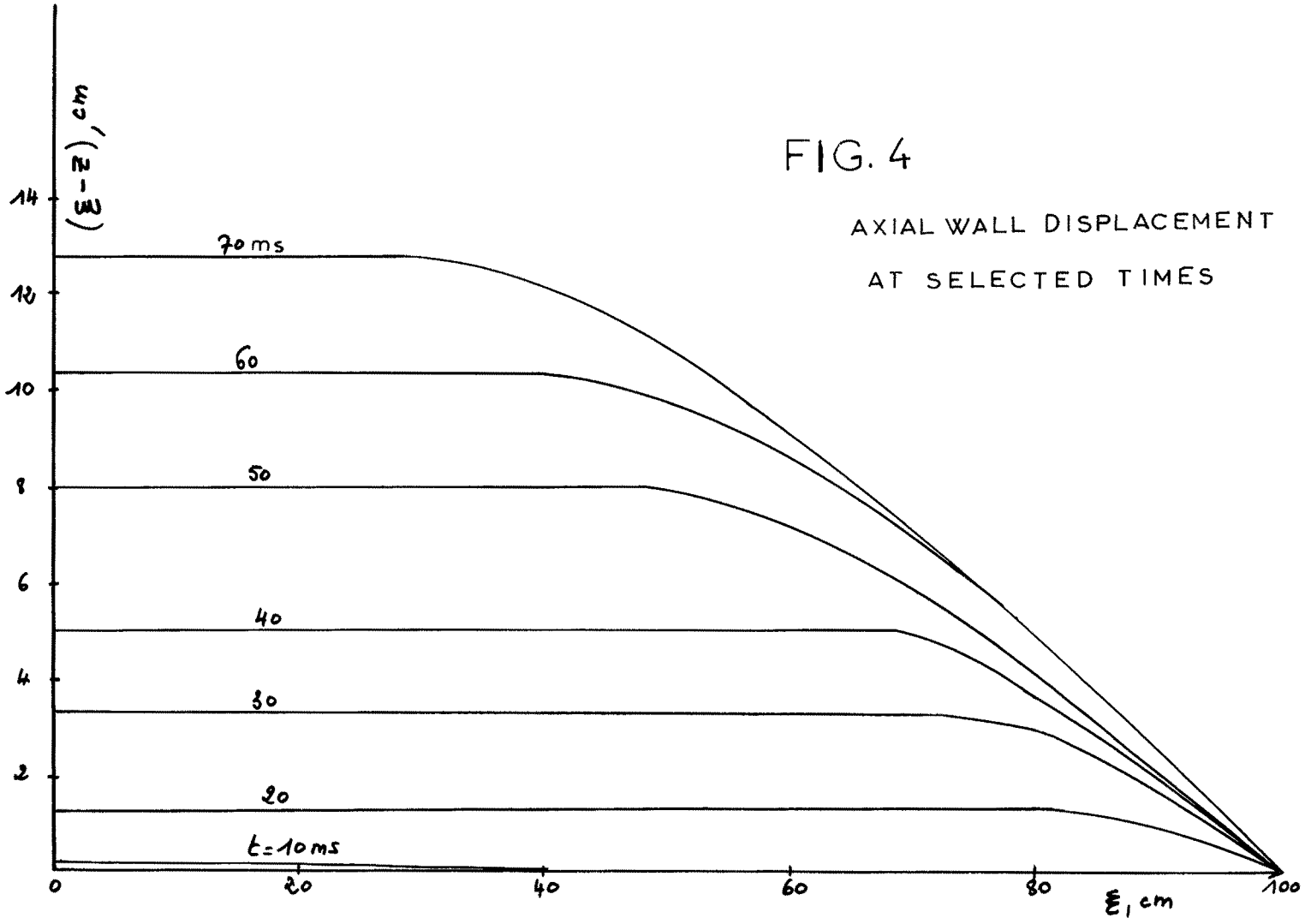

FIG. 5. FLUID VELOCITY AT SELECTED TIMES

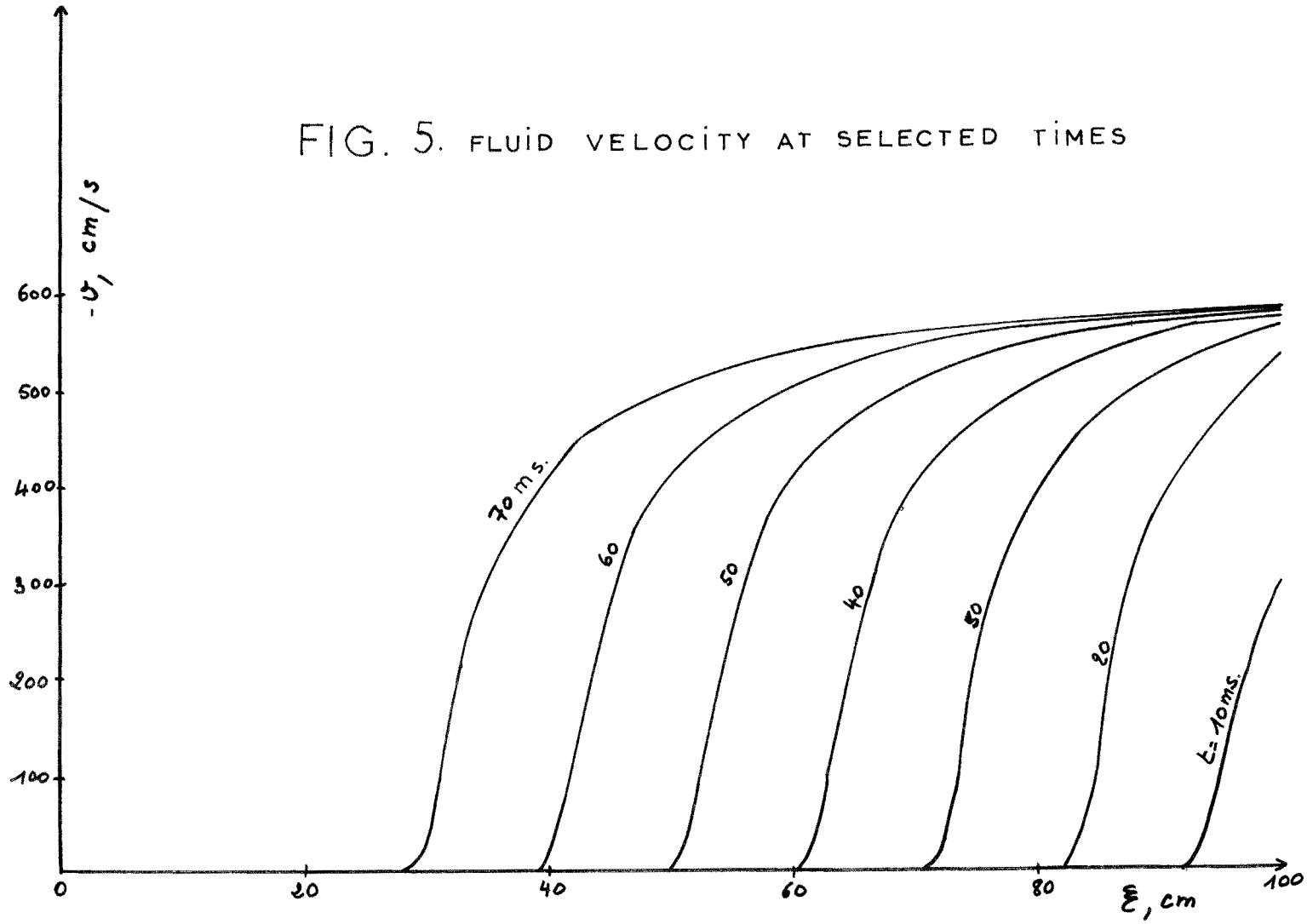

FIG.6

LONGITUDINAL EXTENSION

AT SELECTED TIMES

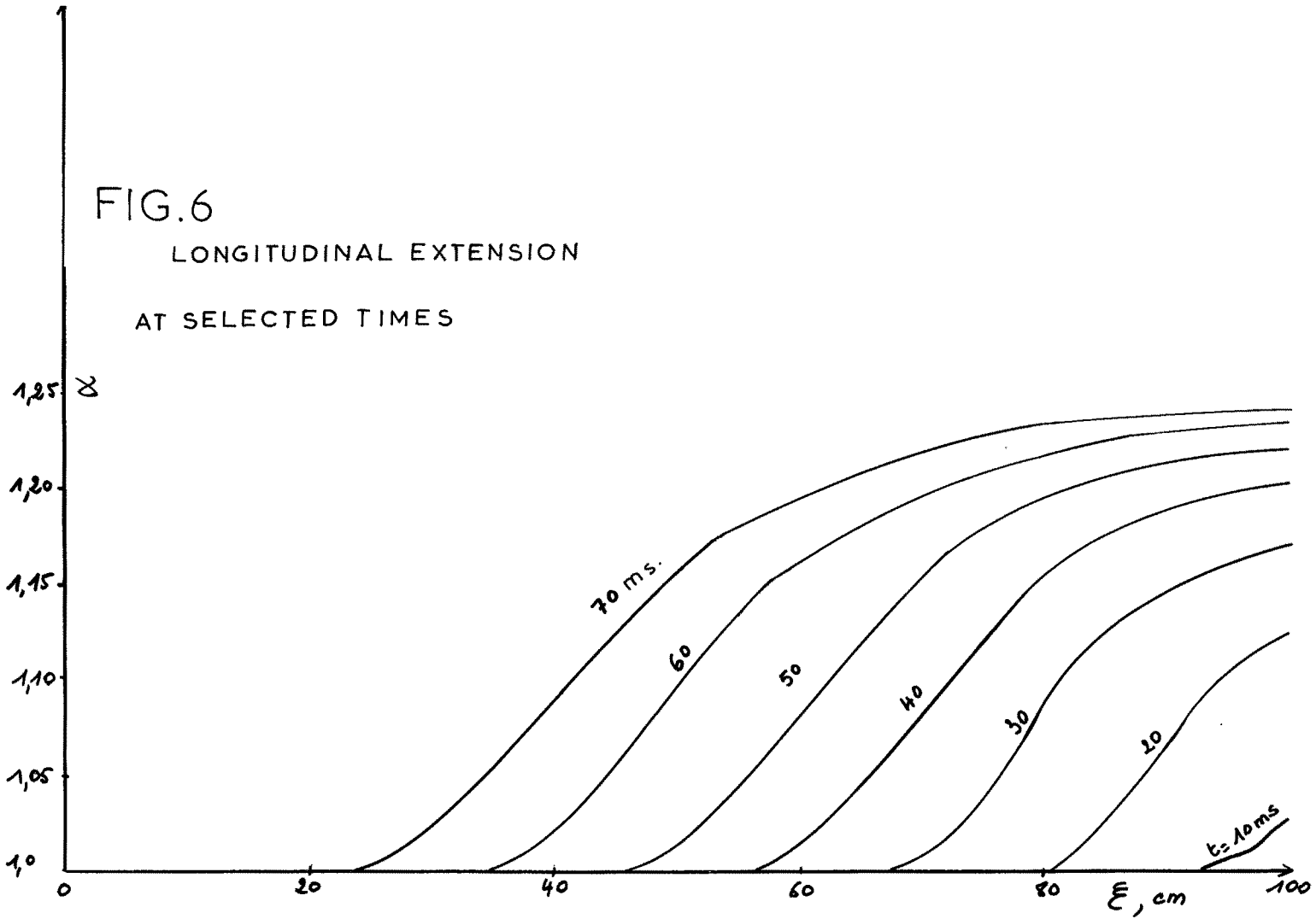

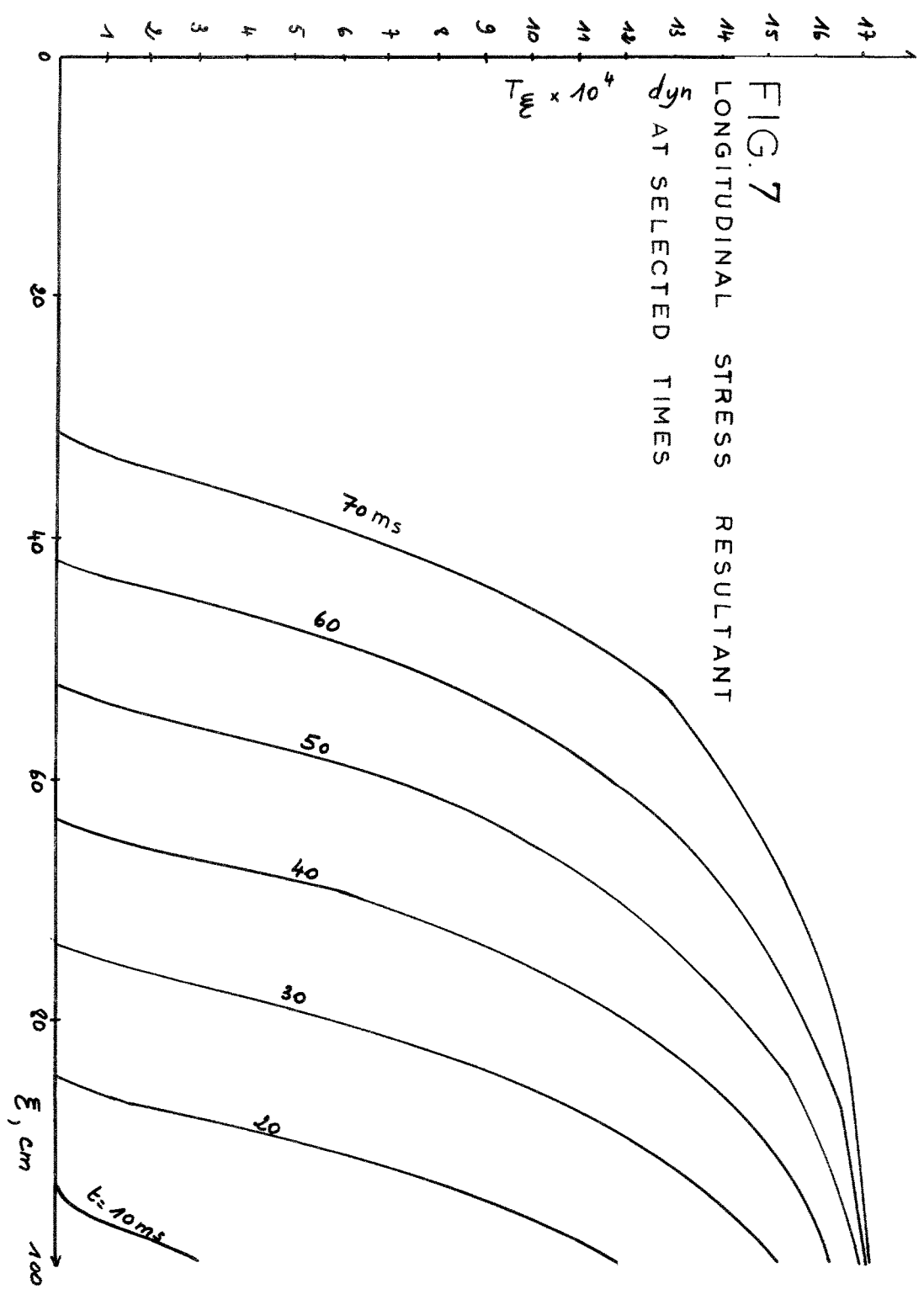
FIG. 7
LONGITUDINAL STRESS RESULTANT
AT SELECTED TIMES
$T_{\xi\xi} \times 10^4$ dyn
70 ms
60
50
40
30
20
t = 10 ms
ξ, cm

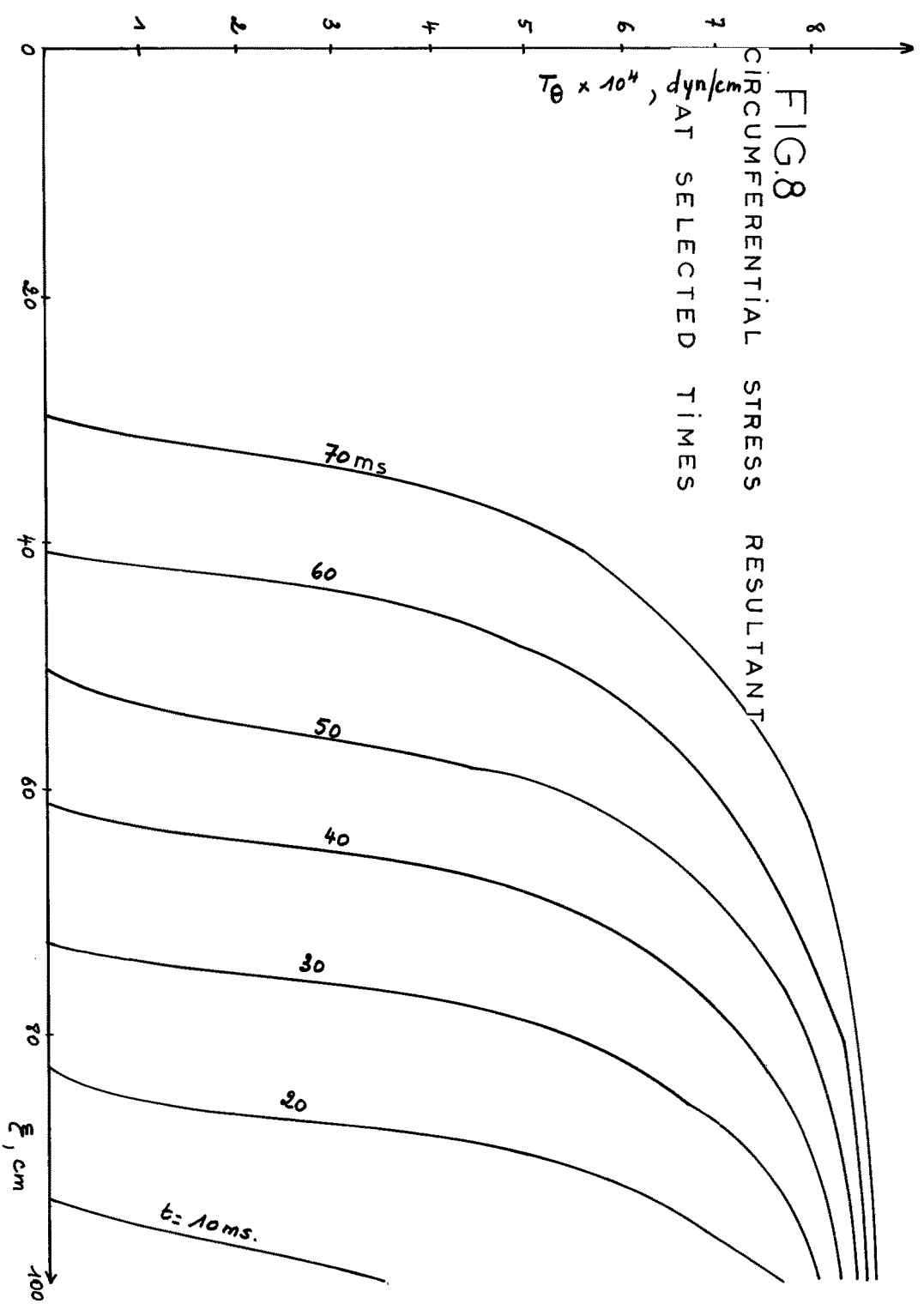

FIG.8
CIRCUMFERENTIAL STRESS RESULTANT
AT SELECTED TIMES